

the ratio of α centers to F centers were to increase in materials containing high concentrations of lead a decrease in F colorability would be observed. It is not unreasonable to expect large concentrations of lead to increase the α center/ F center ratio since lead is an electron trap and, moreover, produces a radiation luminescence²⁵ in the L_1 band region²⁶ causing ionization of F centers. The α -band data presented in Fig. 10 for two of our samples show that the relative α -center production does indeed increase in heavily lead-doped KCl. The percentage of alpha centers produced is comparable to the difference between the curves for 100 ppm and >150 ppm lead shown in Fig. 3.

Our explanation of the experimental results can be summarized briefly. Small or moderate amounts of lead impurity increase the net point defect production in KCl at 80°K by stabilizing radiation produced

²⁵ M. F. Trinkler, *Opt. Spectry*, **16**, 464 (1964).

²⁶ F. Lüty, *Z. Physik* **160**, 1 (1960).

interstitials, thus preventing them from recombining with vacancies. When sufficient lead is present to stabilize all interstitials created by the radiation, no further enhancement of the net vacancy production is observed. In fact, because of the increase in the α center to F -center ratio with increasing lead content, an apparent decrease in F -center production efficiency appears when large concentrations of lead are present in the KCl.

ACKNOWLEDGMENTS

We are grateful to R. B. Murray for his assistance, and for the loan of a cryostat. The use of the electron irradiation facility was made possible by J. A. Ghormley, and the gracious contribution of phosphate glass dosimeters by V. H. Ritz greatly simplified our measurements of radiation absorption. We would also like to thank J. H. Crawford, Jr., for a number of helpful discussions and suggestions.

Alkali-Ion Desorption Energies on Polycrystalline Refractory Metals at Low Surface Coverage*

O. K. HUSMANN

Hughes Research Laboratories, Malibu, California

(Received 18 January 1965; revised manuscript received 18 June 1965)

Alkali-ion desorption energies have been measured under clean surface conditions as monitored by the electron work function. The average surface lifetimes of adsorbed alkali ions have been observed by pulsed desorption following diffusion through the porous metal. About 3 orders of magnitude of surface lifetimes have been investigated. For polycrystalline rhenium, tungsten, molybdenum, and tantalum, the cesium-ion desorption energies are expressed by $Q_i = 0.722(\phi - I) + 1.47$, and for cesium, rubidium, potassium, and sodium on tungsten, by $Q_i = 2.115 - 0.315(\phi - I)$, both in electron volts (within ± 0.05 eV), with ϕ the work function and I the ionization potential. The tungsten-alkali data are in reasonable agreement with the sum of the quantum-mechanically corrected image-charge expression and van der Waals-type interaction. If the change in surface coverage with current density is considered, the alkali-ion desorption energies measured by critical temperature for ion desorption are in tolerable agreement with the above data.

INTRODUCTION

ALKALI-ION and -atom desorption energies have been reported by various investigators¹⁻⁷ over the past three decades. In addition, a number of theoretical approaches to the interpretation of the

desorption energy have been published.⁸⁻¹³ The average lifetime of adsorbed alkali atoms and ions strongly depends on the condition of the substrate surface, its patch distribution, its adsorbed gas layers, and the bulk contamination of the substrate. In the case of oxygen or pyrolytic graphite on the emitter surface, an increased desorption energy has been observed in connection with the increased critical temperature for surface ionization.

Today only a limited number of alkali-ion desorption

* Work supported by NASA-Lewis Research Center Contract NAS 3-4110.

¹ M. D. Scheer and J. Fine, *J. Chem. Phys.* **37**, 107 (1962).

² M. D. Scheer and J. Fine, *J. Chem. Phys.* **38**, 307 (1963).

³ M. D. Scheer and J. Fine, *J. Chem. Phys.* **39**, 1752 (1963).

⁴ F. L. Hughes and H. Levinstein, *Phys. Rev.* **114**, 1023 (1959).

⁵ D. G. Worden in *Progress in Astronautics and Rocketry* (Academic Press Inc., New York, 1961), Vol. 5, p. 141.

⁶ L. H. Taylor and D. G. Worden, *Bull. Am. Phys. Soc.* **8**, 621 (1963); M. S. Kaminsky, *ibid.* **10**, 432 (1965); G. Popp, *Ann. Physik* **13**, 115 (1964).

⁷ F. Knauer, *Z. Physik* **125**, 278 (1948); R. G. Evans, *Proc. Roy. Soc. (London)* **A139**, 604 (1937); T. H. Bull and D. G. Marshall, *Nature* **167**, 478 (1951).

⁸ J. E. Lennard-Jones, *Trans. Faraday Soc.* **28**, 333 (1932).

⁹ N. N. Avgul, A. V. Kiselev, A. I. Lygina, and D. P. Poshkus, *Bull. Acad. Sci. USSR, Div. Chem. Sci.* **23**, 1155 (1959).

¹⁰ I. Higuchi, T. Ree, and H. Eyring, *J. Am. Chem. Soc.* **79**, 1330 (1957).

¹¹ D. P. Stevenson, *J. Chem. Phys.* **23**, 203 (1955).

¹² J. D. Levine and E. P. Gyftopoulos, *Surface Sci.* **1**, 176 (1964).

¹³ L. J. Varnerin, *Phys. Rev.* **91**, 859 (1953).

energies measured on the refractory metals rhenium, tungsten, and molybdenum are available. All except those for rubidium on tungsten result from polycrystalline surfaces. It is the purpose of this paper to add ion desorption-energy data to those already known and to contribute to their theoretical interpretation.

THEORETICAL EVALUATION

In this theoretical evaluation, classical calculations of the interaction between a charged, rare-gas-configuration ion with an idealized conducting plane is considered (12-1 potential).¹⁴ Owing to the small distance between this conducting plane and the adsorbed ion, later the image-force term is quantum-mechanically corrected. Besides the 12-1 potential, a second approach takes account of the corrected image force and a term proportional to the ion polarizability as derived by application of perturbation theory. The ion desorption energy $Q(r)$ (method I) results from the sum of repulsive Q_{rep} , image Q_{im} and polarization Q_{pol} energies.

$$Q(r) = Q_{\text{rep}} + Q_{\text{im}} + Q_{\text{pol}}, \quad (1)$$

where

$$Q_{\text{rep}}(r) = (\epsilon_0/2)(r_0/r)^{12}, \quad (1a)$$

$$Q_{\text{im}}(r) = -e^2/4r, \quad (1b)$$

$$Q_{\text{pol}}(r) = [2\alpha/(2r)^3]Q_{\text{im}}(r). \quad (1c)$$

$dQ(r)/dr=0$ yields the ion-to-substrate distance; α is the ion polarizability. The inert-gas atoms and the alkali ions have the same outer-shell configuration. For ϵ_0 , therefore, those inert-gas coefficients have been used which correspond best to the alkali ions (see Table I, second column).¹⁵ $\epsilon_0/2$ is employed in the calculations because in this case one ion interacts with the substrate atoms, rather than each alkali ion interacting with the other. The third column of Table I shows the inert-gas interatomic distances.¹⁵ Column 4 shows measured alkali-ion polarizabilities (averages from publications).¹⁶

It is recognized that the image-charge expression

TABLE I. 12-1 potential constants.

1	2	3	4
Inert gas	ϵ_0 ergs ^a	Interatomic distance Å	Alkali-ion polarizability α , Å ³
Xe(Cs ⁺)	309.9	4.56	2.73
Kr(Rb ⁺)	238.4	4.03	1.64
Ar(K ⁺)	165	3.84	1.01
Ne(Na ⁺)	48.2	3.12	0.21

^a ϵ_0 is in units of 10^{-16} ergs.

¹⁴ J. A. Becker, Ann. N. Y. Acad. Sci. 58, 723 (1954).

¹⁵ American Institute of Physics Handbook (McGraw-Hill Book Company, Inc., New York, 1963), 2nd ed., Chap. 4, paragraph 170.

¹⁶ R. M. Sternheimer, Phys. Rev. 115, 1198 (1959).

TABLE II. Refractory metal lattice constants.

	Lattice constant Å	Structure type
Re	2.755	Hexagonal close
W	3.158	Cubic body
Mo	3.14	Cubic body
Ta	3.29	Cubic body

needs a quantum-mechanical correction for distances less than a few angstroms. This correction can be expressed by¹⁷

$$Q_{\text{im-corr}} = \xi \kappa^{1/2} (e^2/4r^2) \quad (2)$$

when the quantum-mechanical problem of the interaction of a charged macroscopic body with a metal surface is treated by means of the variation method. The corrected image-charge term is

$$Q_{\text{im}}^*(r) = -(e^2/4r) + \xi \kappa^{1/2} (e^2/4r^2) \quad (2a)$$

with

$$\kappa \approx -\frac{1}{3} \left(\frac{3}{8\pi} \right)^{1/3} \rho^{-2/3} + \frac{(2\pi)^2}{6} \left(\frac{3}{8\pi} \right)^{2/3} \frac{\hbar^2}{me^2} \rho^{-1/3}.$$

The constant ξ depends on the choice of wave function used in deriving Eq. (2). According to Sachs and Dexter,¹⁷ the upper limit for ξ is 0.46 and according to Cutler *et al.*,¹⁸ its lower limit is 0.09. Since no definite value exists, ξ is derived here by matching the calculated with the measured sodium-ion desorption energy. The sodium-ion desorption energy is selected because of the small sodium-ion polarizability.¹⁹ Geometrical considerations for sodium on the tungsten (110) plane also lead to $\xi=0.33$.¹⁹ Consequently, $\xi=0.33$ is used for the polycrystalline surface considered here.²⁰ ρ is the number of free electrons per unit volume in the metal. There is approximately one free electron per lattice atom, and the free-electron density depends on the lattice constant and the structural type of the lattice (see Table II). The substrate only weakly influences the ion desorption energy in terms of ρ .

The second approach (method II) takes into account the corrected image force [Eq. (2a)] and the ion polarizability, with the latter interaction expressed by Eq. (3a), according to application of the perturbation theory (Prosen *et al.*).²¹ In this approach, the short-range repulsive force is not considered. If we assume that the repulsive force decreases more strongly than with the 12th power, its contribution is small. In addition, Avgul *et al.*,⁹ have shown that dipole-quadrupole and quad-

¹⁷ R. G. Sachs and D. L. Dexter, J. Appl. Phys. 21, 1304 (1950).

¹⁸ P. H. Cutler and J. J. Gibbons, Phys. Rev. 111, 394 (1958).

¹⁹ H. E. Neustadter and K. P. Luke, NASA TN D 2460, 1964 (unpublished).

²⁰ With $\xi=0.33$, the 12-1-potential ion radii are for Cs, Rb, K, and Na in the same sequence 1.783, 1.533, 1.426, and 1.063 Å.

²¹ E. J. R. Prosen and R. G. Sachs, Phys. Rev. 61, 65 (1942).

TABLE III. Calculated desorption energies (values in eV).

1	2	Method I		Method II		
		3	4	5	6	7
	Q_{im}	12-1 Potential Q total uncorr	12-1 Potential Q total qm-corr	Q_{im}^*	Q_{pol}	Q_{total}
Cs ⁺	-2.18	-2.12	-1.688	-1.703	-0.204	-1.907
Rb ⁺	-2.415	-2.45	-1.891	-1.835	-0.1373	-1.975
K ⁺	-2.70	-2.61	-1.953	-1.975	-0.0944	-2.07
Na ⁺	-3.67	-3.56	-2.292	-2.32	-0.025	-2.345

drupole-quadrupole terms are not negligible and tend to cancel the repulsion term.

$$Q_{total}(r) = +Q_{im}^*(r) + Q_{pol}(r), \quad (3)$$

$Q_{im}^*(r)$ is identical with that given by Eq. (2a)

$$Q_{pol}(r) = -\frac{\alpha e^2 \pi (3\pi^2 \rho)^{2/3} \ln[2(3\pi^2 \rho)^{1/3} r]}{(2\pi)^3 r^2} \quad (3a)$$

where r is the Pauling ion radius and $e = 1.6 \times 10^{-19}$ C.

Table III combines the calculated ion desorption energies, following from methods I and II. The image-charge term is added for comparison. Considered for these calculations is an idealized polycrystalline surface with random patch distribution, and ξ and ρ are applied to this surface. The second column presents $Q = e^2/r$; the third (method I), the desorption energy according to the 12-1 potential with uncorrected image force. Column 4 (method I) shows the 12-1 potential with quantum-mechanically-corrected image force. Columns 5 and 6 result from Eqs. (2a) and (3a) and column 7 presents the ion desorption energies according to Eq. (3). Comparison of the second and third columns reveals close agreement between desorption energies resulting from the image force and the 12-1 potential because of partial compensation of the repulsive and polarization forces. The 12-1 potential data for corrected image force (column 4) compare better with measured data and come closer to the data obtained with method II (column 7).

EXPERIMENTAL EVALUATION

The standard technique for measuring ion and atom desorption energies is the pulsed-molecular-beam method, which takes into account the exponential dependence of the average surface lifetime upon desorption energy. This is expressed by the Frenkel equation with the average surface lifetime in seconds

$$\tau = \tau_0 \exp(Q/kT), \quad (4)$$

where Q is the desorption energy in eV and T the absolute temperature. In the experiments reported here, the alkali ion is removed from the emitter surface by the pulsed acceleration potential after diffusion through the porous pellet. The exponential ion-current decay is

photographically recorded with a Tektronix 545A oscilloscope. The oscilloscope time-base calibration was compared with the 60-cps power-line frequency and deviations of less than 2% were measured. Linearity of the vertical amplifier was within 2%. The average surface lifetime results from

$$i/i_0 = 1/e \quad (\text{where } e = 2.718) \quad (5)$$

with i_0 an arbitrary point on the decay slope.⁷ Only the exponentially decaying part is considered. The acceleration-potential pulse frequency is adjustable between 5 and 50 pulses/sec and the pulse width is continuously adjustable between 100 and 1000 μ sec; the rise time is at most 2% of the pulse width. The acceleration potential is kept constant at 10 kV, and the alkali flow adjusted to yield less than a monolayer of emitter surface coverage between the pulses. Sintering of the porous material during the time of experimentation is negligible.²² The pellet transmission coefficient has been measured with helium in the operating temperature range and is close to 10^{-4} for all pellets investigated.²³ (The transmission coefficient is the ratio of the number of atoms leaving after diffusion to the number impinging on the back side of the emitter.) The pellets are electron-beam-welded to a molybdenum support.

The porous emitter has an average surface area of 0.25 cm², is of concave shape, and is incorporated into a Pierce-gun-type electrostatic acceleration structure. The gun permeance for cesium ions is 3×10^{-9} A/volt^{3/2}. The extraction potential applied here is above the space-charge limit and the field strength on the emitter surface is 14 kV/cm.²⁴ At this field strength, the Schottky effect is small. The desorption energy is lowered because of the term $(e^3 E)^{1/2}$. This yields, at $E = 14$ kV/cm, a reduction in the ion desorption energy by 0.045 eV, well inside the stated error limit.

Electrolytic-tank studies on a typical porous metal surface with a pore diameter and pore depth of 1 μ and a pore distance of 2 μ yielded 1.4 kV/cm for the pore center and 10 kV/cm close to the pore rim with 10-kV acceleration potential. The field at the pore rim depends on its curvature. Here fields in excess of 10^5 V/cm are not very probable. Ion emission from this area is limited owing to its size and to ion migration. Preliminary ion-microscope studies of ion emission from a single pore confirmed, for cesium on tungsten as an example, migration lengths in the range from 1 to 2 μ , with moderate temperature dependence.

Figure 1 is a cross section of the ion-gun-Faraday-cage assembly. The lower portion of the ion gun consists of the alkali supply tube which is closed by the porous pellet. The Faraday cage is located opposite the ion gun; it is liquid-nitrogen-cooled during operation and is positive-biased with respect to the accelera-

²² O. K. Husmann and R. R. Turk, AIAA J. (to be published).

²³ O. K. Husmann in *Progress in Astronautics and Rocketry* (Academic Press Inc., New York, 1961), Vol. 5, p. 505.

²⁴ T. VanDuzer and G. R. Brewer, J. Appl. Phys. 30, 291 (1959).

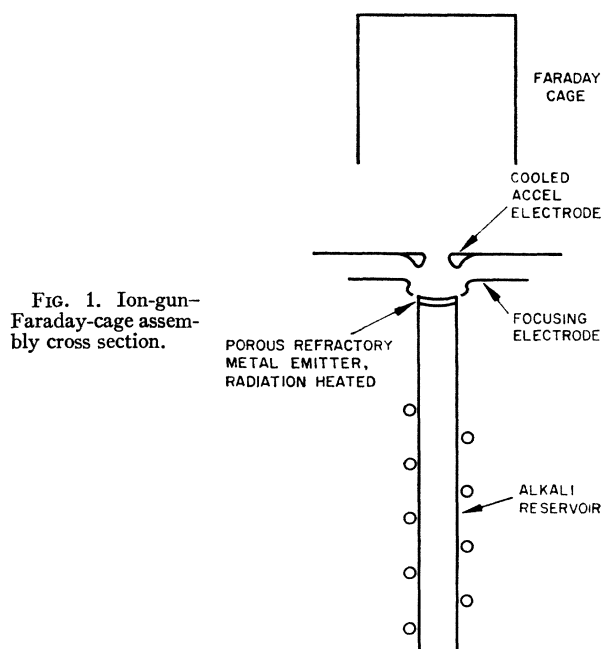


FIG. 1. Ion-gun-Faraday-cage assembly cross section.

tion electrode to avoid secondary-electron emission. The acceleration electrode itself is water-cooled and maintained at about 300°K. Ion-beam interception by this electrode, and therefore secondary-electron emission, is negligible, as demonstrated by electrolytic-tank studies.²⁴ Secondary electrons produced by charge-exchange ions upon impact on the acceleration electrode contribute less than 0.1% to the Faraday-cup current.

The ion-lifetime measurements were expanded over temperatures ranging from 1100 to 1500°K (controlled by a Leeds and Northrup pyrometer). The spectral emissivities of the various porous materials were measured by comparing the surface temperature with that in a hole 0.22 in. deep and 0.03 in. in diameter. They are: rhenium, 0.47; tungsten, 0.6 (average); molybdenum, 0.55; tantalum, 0.55.²⁵ No temperature gradient exists on the indirectly heated 0.22-in.-diam pellets. The emitter temperatures are accurate to within 8°K.

In order to maintain clean surface conditions during operation, the system is equipped with a 200-liter/sec ion pump, and pressures in the low 10^{-9} Torr range are standard. The residual-gas atmosphere is monitored by a calibrated CEC 21-612 mass analyzer with 1×10^{-9} Torr/division sensitivity for oxygen at 100 μ A electron current. Prior to ion-pump operation, the system (including the ion pump) is baked for 12 h at 150°C, evacuated by a mercury diffusion pump, and protected against backstreaming hydrocarbons from the mechanical pump by a zeolite trap. All seals are copper gaskets. Cleanup of the emitter surface is checked by the electron work function, with current densities

covering three to four orders of magnitude.²⁶ The first measurements after baking mostly yield high values, and in the low-temperature region the residual gas atmosphere turns the slope toward higher work functions. At pressures below 10^{-8} Torr the remaining problems are surface cleanup and removal of bulk contaminants. (After shutoff of the ion pump for a few hours, only small increases of the mass numbers 2 and 28 were noticed.) No change in work function was registered during such periods. Flashing of the emitter from room temperature up to about 1750°K after sufficient exposure to the residual-gas atmosphere yields a small increase in pressure, but no increase was noticed with the emitter above 1000°K prior to flashing. For most of the residual gases, the heat of desorption is low and the sticking probability in the temperature range under consideration is negligible.²⁷⁻²⁹ An exception is oxygen. It is reported to desorb from tungsten at about 1800°K.³⁰ Here in general a clean-surface work function was measured after high-temperature treatment ($\sim 1600^\circ\text{K}$) with simultaneously a small alkali flow through the emitter, usually over several hours. Carbon is one of the frequent contaminants in tungsten, molybdenum, and tantalum, and its presence is indicated by a reduced work function.³¹ In the case of emitter carburization, first oxygen was admitted at partial pressures up to 10^{-4} Torr with the emitter close to 1600°K. The CO peak simultaneously was monitored until its disappearance. Subsequently, oxygen was removed according to the above schedule. The final work functions agree closely with accepted values for the polycrystalline surfaces (if the Richardson constant is $A = 120 \text{ A/deg}^2 \text{ cm}^2$) and remain stable over the time of operation. These ϕ are for Re, W, Mo, and Ta, respectively, 4.9, 4.54, 4.24, and 4.15 eV. In the case of tungsten, as an example, the resolution makes it difficult to distinguish between $\phi = 4.49 \text{ eV}$ with $A = 90$ and $\phi = 4.54 \text{ eV}$ with $A = 120$. Alkalies (such as cesium in the sodium reservoir) may affect the average Na surface lifetimes. For this reason, the alkali ampules were checked spectroscopically. A typical analysis shows 16 ppm sodium, 16 ppm potassium, and 24 ppm rubidium, in addition to traces of alkaline-earth and other elements in cesium. Approximately the same order of magnitude of alkali contaminants has been found in rubidium, potassium, and sodium.

²⁶ During work function measurements, the ion-gun electrodes are free from alkalies. The Mo focusing electrode temperature is more than 300°K below emitter temperature.

²⁷ R. Gomer, R. Wortman, and R. Lundy, *J. Chem. Phys.* **26**, 1147 (1957); E. W. Mueller, *Ergeb. Exakt. Naturw.* **27**, 290 (1963); J. Eisinger, *J. Chem. Phys.* **29**, 1154 (1958).

²⁸ R. Suhrmann, *Z. Electrochem.* **60**, 804 (1956); J. Eisinger, *J. Chem. Phys.* **28**, 165 (1958).

²⁹ J. Eisinger, *J. Chem. Phys.* **27**, 1205 (1957).

³⁰ J. A. Becker, E. J. Becker, and R. G. Brandes, *J. Appl. Phys.* **32**, 411 (1961).

³¹ O. K. Husmann, D. M. Jamba, and D. R. Denison, *AIAA Paper No. 64-693*, 1964 (unpublished).

²⁵ O. K. Husmann, *AIAA J.* **1**, 2607 (1963).

In separate experiments,³² the effects of 10% of one additive mixed with cesium were studied with regard to work function and critical temperature. After two months of continuous operation, no effects have been detected in the cases of barium and calcium additives. With rubidium, potassium, and sodium, however, the original cesium critical temperatures shifted toward those of the additives.

For the data reported here, the average surface lifetimes were measured over approximately one week to insure the absence of alkali contaminants in the reservoir.

EXPERIMENTAL RESULTS

After emitter cleanup, the alkali-ion desorption energies were measured on rhenium, tungsten, molybdenum, and tantalum. These data are compiled in Table IV. (The error limit for desorption energies is

TABLE IV. Measured ion desorption energies.

	Rhenium		Tungsten		Molybdenum		Tantalum	
	Q_i eV	τ_0 10^{-18} sec	Q_i	τ_0	Q_i	τ_0	Q_i	τ_0
Cs ⁺	-2.2	11.4	-1.95	17.7	-1.72	12.3	-1.65	1.8×10^4
Rb ⁺			-2.07	3.4			-1.81	236
K ⁺			-2.22	2.3			-2.05	41.6
Na ⁺			-2.33	6.3				

± 0.05 eV.) In accordance with the energy diagram, the desorption energies given are negative. Table V presents the alkali surface lifetimes at 1100 and 1500°K.

These alkali-ion desorption energies are lower than those reported in Table III, column 2 in connection with the image force. It is interesting to note the good agreement between the measured ion desorption energies on tungsten and those computed according to Eq. (3). (See Table III, column 7.)

In curves *A* and *B* of Fig. 2, the measured ion desorption energies are plotted versus the difference between work function ϕ and ionization potential I in relation to the Schottky equation,¹⁴

$$Q_a - Q_i = e(\phi - I) - dQ \quad (6)$$

with Q_a the atom desorption energy and dQ the ionization activation energy. For comparison, computed ion desorption energies are added and curves *C* and *D* are calculated according to the second method. We notice a steadily decreasing ion desorption energy from rhenium to tantalum. The ion desorption energies for tantalum (in agreement with those for tungsten) increase from cesium through rubidium to potassium (see Table IV). This agrees well with the trend of the image force.

The τ_0 data for rhenium, tungsten, and molybdenum

³² O. K. Husmann, Final Report on Contract NAS 3-4110 (unpublished).

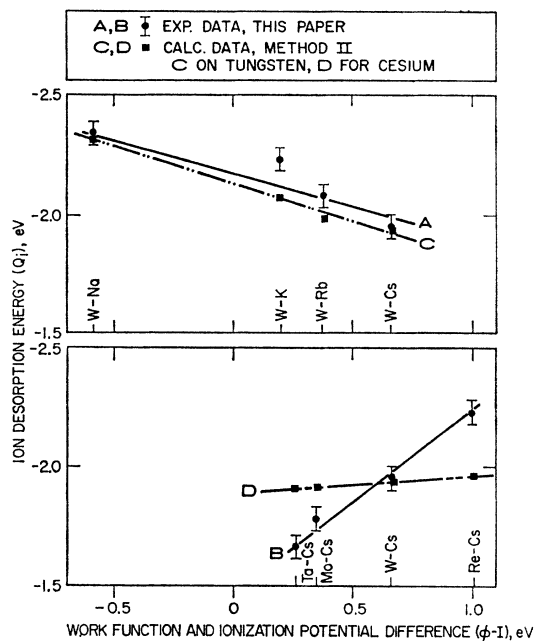


FIG. 2. Alkali-ion desorption energies and their theoretical interpretation.

are in good agreement with theoretical considerations.³³⁻³⁵ However, those measured on tantalum (particularly with cesium) are much longer. It should be emphasized that the tantalum electron work function for these measurements was 4.15 eV. It is interesting to note that the critical temperature for cesium on tantalum exceeds that on rhenium.²⁵

ION DESORPTION ENERGY AND CRITICAL TEMPERATURE

At low electric field, the critical temperature for surface ionization depends on the ion current density. It is defined by the steep increase of ion current to its saturation due to clean up of the emitter surface from excessive alkali.³⁶ With the Frenkel equation (4), the desorption energy is

$$Q_i = (k/e) \frac{T_2 \cdot T_1}{T_2 - T_1} \ln \frac{\tau_1}{\tau_2} \quad (7)$$

and with

$$\tau = \frac{\theta \sigma_0 e}{j}, \quad (8)$$

³³ S. Glasstone, K. J. Laidler, and H. Eyring in *The Theory of Rate Processes* (McGraw-Hill Book Company, Inc., New York, 1941).

³⁴ J. H. DeBoer in *The Dynamical Character of Adsorption* (Clarendon Press Inc., Oxford, 1953).

³⁵ J. D. Levine and E. P. Gyftopoulos, *Surface Sci.* **1**, 225 (1964).

³⁶ O. K. Husmann in *Progress in Astronautics and Aeronautics* (Academic Press Inc., New York, 1963), Vol. 9, p. 195.

TABLE V. Average surface lifetimes in seconds.

	Rhenium		Tungsten		Molybdenum		Tantalum	
	1100°K	1500°K	1100°K	1500°K	1100°K	1500°K	1100°K	1500°K
Cs ⁺	1.43×10 ⁻²	9.93×10 ⁻⁶	1.54×10 ⁻³	2.5 ×10 ⁻⁶	9.76×10 ⁻⁶	3.28×10 ⁻⁷	6.68×10 ⁻²	2.85×10 ⁻⁴
Rb ⁺			1.05×10 ⁻⁴	1.15×10 ⁻⁷			4.7 ×10 ⁻³	1.18×10 ⁻⁵
K ⁺			3.48×10 ⁻³	2.3 ×10 ⁻⁶			1.05×10 ⁻²	1.2 ×10 ⁻⁵
Na ⁺			3.15×10 ⁻³	1.47×10 ⁻⁵				

we get

$$Q_i = (k/e) \frac{T_2 \cdot T_1}{T_2 - T_1} [\ln(j_2/j_1) - \ln(\theta_2/\theta_1)], \quad (9)$$

where T is the emitter temperature, j the ion current density, and θ the surface coverage relative to a monolayer. σ_0 is the number of atoms per cm² in a monolayer. Equation (9) contains the logarithm of the change in surface coverage with current density. In column 4 of Table VI, the ion desorption energies are computed according to Eq. (9) from critical-temperature data, assuming $\theta_2/\theta_1 = 1$. These desorption energies exceed those reported in Table IV. If the change in surface coverage is considered [using ion desorption energies from Table IV in connection with Eq. (8)], then critical-temperature ion desorption energies come closer to those reported in Table IV (see last column in Table VI).

At current densities below 0.1 mA/cm², the critical temperatures measured on porous emitters correspond to those of the solid material.²⁶ T_c can be expressed by an equation of the form

$$T_c = A / (B - \log j) \quad (10)$$

with T_c in degrees Kelvin and j in amperes per square centimeter.

TABLE VI. Critical-temperature data.

	A	B	Q_i (eV)	$Q_i(\theta)$ (eV)
Cs ⁺	14.0×10 ⁸	8.764	-2.73	-1.94
Rb ⁺	14.1×10 ⁸	8.54	-2.76	-1.965
K ⁺	16.3×10 ⁸	9.69	-2.81	-2.14
Na ⁺	16.3×10 ⁸	9.19	-3.26	-2.26

For the four alkalis under consideration, the equation constants A and B (tungsten) are given in Table VI.

CONCLUSIONS

The measured alkali-ion lifetimes on porous tungsten are in good agreement with computed data which take into account the quantum-mechanically-corrected image force and the polarization force (method II, Table III). With the corrected image force, the 12-1-potential alkali-ion desorption energy comes closer to the experimental data.

In all our experiments, clean surface conditions were maintained and checked by the thermionic work function. All measurements were done on polycrystalline surfaces. Surface contaminants, which may severely influence the average surface lifetimes, have been removed either by applying high temperatures and small amounts of alkali or by oxygenation of the surface.

The constant τ_0 in the Frenkel equation measured on tantalum exceeds the expected range of 10⁻¹² sec, particularly in the case of cesium. The desorption energies, however, in accordance with those measured on tungsten, increase from cesium to potassium.

ACKNOWLEDGMENTS

The author would like to acknowledge the help of Dr. R. Kikuchi of this laboratory who handled the computer calculation of the 12-1 potential. Individual thanks are also extended to D. Jamba for the mass-spectrometer calibration and critical-temperature measurement with contaminated cesium, and to J. Becker and J. Mullane for their help in building the equipment.